JOURNAL OF COMPUTATIONAL PHYSICS 115, 423–430 (1994)

Transient Conjugated Heat Transfer Analysis from a Sphere with Nonlinear Boundary Conditions

SEUNGHO PAIK* AND HOA D. NGUYEN

Idaho National Engineering Laboratory, EG & G Idaho, Inc., Idaho Falls, Idaho 83415

AND

JACOB N. CHUNG

Department of Mechanical and Materials Engineering, Washington State University, Pullman, Washington 99164-2920

Received June 26, 1992

The problem of conjugate unsteady convective and radiative heat transfer from a solid spherical particle is numerically investigated for Reynolds numbers up to 100 using a Chebyshev–Legendre spectral method. The treatment of nonlinear boundary condition of the radiation heat transfer from the sphere surface is assessed and successfully implemented. This work is an extension of the previous effort of simulating flow around a sphere using spectral method to include heat transfer. The assumption of quasi-steady flow field for the unsteady heat transfer calculation is compared with the fully transient treatment of both the flow and the temperature fields. It is found that the quasi-steady assumption underestimates the overall heat transfer rate at very early time stages (up to 9% underestimation for the mean Nusselt number). However, the discrepancy becomes smaller as time elapses. The underprediction of the quasi-steady assumption becomes larger as the Reynolds number increases for a fixed Prandtl number. The results for different alternate radiation–conduction number cases are presented.

1. INTRODUCTION

There has been a constant need for research into the fluid flow and heat transfer about a rigid sphere because of its extensive applications [1]. Both experimental and theoretical studies have been conducted to examine the various effects of a spherical particle exposed to a convective environment. On the theoretical side, several numerical models with varying levels of complexity have been constructed to address various issues of thermal transport associated with a spherical particle. One of the approaches uses a quasi-steady model where momentum transport is assumed to be a steady process, while heat transfer is considered to be transient [1]. However, the transient behavior of the sphere predicted by this approach becomes questionable, especially in an early time stage. It is well known that for a small Prandtl number momentum transfer takes longer to establish a steady state boundary layer near a solid surface than does heat transfer. A recent study of Nguyen and Chung [2] shows that the flow field of a compulsively started sphere reaches steady state after 15 units of dimensionless time ($=R/U_\infty$, where R is the sphere radius and U_∞ is the free stream velocity) for Reynolds numbers in the range lower than 100. From the time the sphere is exposed to a convective environment, the flow structure changes continuously from a creeping-like flow to a fully developed boundary-layer-type flow [3]. Because of these transient phenomena, the flow and temperature fields obtained by using a quasi-steady hypothesis may deviate from those obtained by fully transient treatment. In order to quantify the difference between the quasi-steady results and fully transient results, it is necessary to solve the momentum and energy conservation equations in a fully transient manner. Another assumption frequently used for analyzing the flow over a sphere is that the sphere has a uniform temperature such that no temperature gradient exists within the body of the sphere. Unless the sphere thermal conductivity is small compared to that of the fluid, this assumption is valid since the sphere will adjust rather quickly to thermal changes of the environment.

The present study is based on the transient, conjugate approach which treats both exterior and interior domains separately in such a way that the temperature and the heat flux of the two domains match at the interface. A fully transient and conjugate model in conjunction with a Chebyshev–Legendre spectral numerical scheme used for the flow simulation [2] is developed to establish a methodological basis upon which extensive evaluation of the two approaches described above is conducted. In addition, a numerical experiment using the influence matrix technique for a nonlinear boundary value problem is performed. Influence matrix technique has been success-

* To whom correspondence should be addressed at: Idaho National Engineering Laboratory, EG & G Idaho, Inc., P.O. Box 1625, MS 3880, Idaho Falls, Idaho 83415.

581/115/2-13

0021-9991/94 $6.00

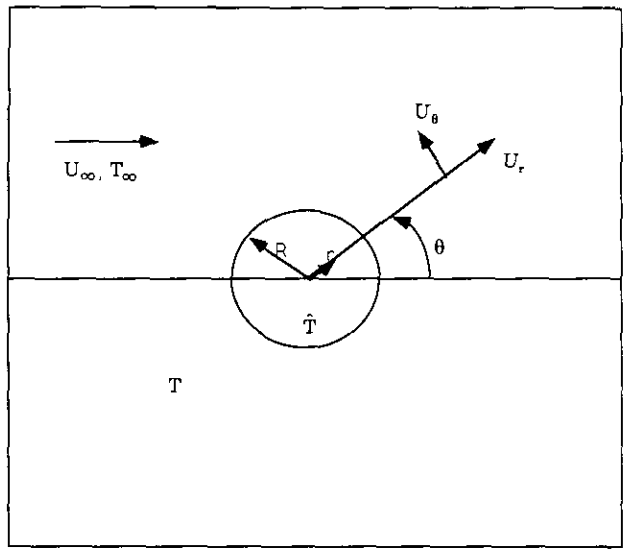

FIG. 1. Schematic of the coordinate system.

fully applied to decomposing the stream function and vorticity for the Navier–Stokes equation [2]. This technique is extended to treat a nonlinear boundary condition such as that encountered in thermal radiation. Results based on the quasi-steady assumption are compared with those obtained by simultaneous treatment of the unsteady momentum and energy conservation equations.

2. MATHEMATICAL FORMULATION

2.1. *Problem Statement*

Figure 1 illustrates the physical configuration and geometry under consideration in the spherical coordinates system (r, θ) with the origin taken to be at the center of the sphere. As depicted, a rigid particle, assumed to be spherical in shape, of radius R and at temperature T_0 is exposed to an unbounded incompressible fluid at temperature T_∞. At the time of exposure ($t = 0$), the motion of the outside fluid is suddenly started in an impulsive fashion such that the flow is instantaneously accelerated from rest to U_∞ going from left to right. For the systems considered here, the temperature is assumed to be low enough that thermal radiation is neglected, and therefore the present analysis precludes high temperature systems such as those in thermal plasma processing, combustion, etc. Within this temperature range, the thermophysical properties are approximately constant and will be assumed valid in this study. Also, it is assumed that the flow and temperature fields are axisymmetric so that no azimuthal variation exists in any dependent variable.

2.2. *Governing Equations*

For the scenario described in the preceding subsection together with the outlined assumptions, the thermal phenomena may be described by a set of equations representing mass, momentum, and energy conservation. In streamfunction–vorticity formulations, the mass and momentum equations may be cast in nondimensional form as

$$\frac{\partial \Omega}{\partial t} - \frac{1}{r}\frac{\partial(\Psi, \Omega/r\sin\theta)}{\partial(r,\theta)} = \frac{2}{\mathrm{Re}}\frac{1}{r\sin\theta}E^2(\Omega r\sin\theta) \tag{1}$$

$$E^2\Psi = -\Omega r\sin\theta, \tag{2}$$

where t and r are time and radial coordinates nondimensionalized as t = time $\times$ $U_\infty/2R$, r = radial length/R. R and U_∞ are the radius of the sphere and free stream velocity, respectively. Re is the Reynolds number based on the sphere's diameter and the free-stream velocity, and Ω and Ψ are the dependent quantities representing vorticity and stream function in respective order, $\partial(\ ,\ )/\partial(\ ,\ )$ is the conventional notation of the Jacobean. The operator E^2 employed in Eqs. (1) and (2) is defined as

$$E^2 = \frac{\partial^2}{\partial r^2} + \frac{\sin\theta}{r^2}\frac{\partial}{\partial\theta}\left(\frac{1}{\sin\theta}\frac{\partial}{\partial\theta}\right). \tag{3}$$

The energy conservation equation outside the sphere without internal heat generation is written in nondimensional form as

$$\frac{\partial Z}{\partial t} + \left[U_r\frac{\partial Z}{\partial r} + \frac{U_\theta}{r}\frac{\partial Z}{\partial\theta}\right] = \frac{2}{\mathrm{Pe}}\left[\frac{\partial^2 Z}{\partial r^2} + \frac{2}{r}\frac{\partial Z}{\partial r} + \frac{1}{r^2\sin\theta}\frac{\partial}{\partial\theta}\left(\sin\theta\frac{\partial Z}{\partial\theta}\right)\right], \tag{4}$$

where Pe is the Peclet number. U_r and U_θ are the r- and θ-direction velocity components defined in terms of the stream function as

$$\{U_r, U_\theta\} = \frac{1}{r\sin\theta}\left\{\frac{1}{r}\frac{\partial\Psi}{\partial\theta}, -\frac{\partial\Psi}{\partial r}\right\}, \tag{5}$$

and Z is the dimensionless temperature defined as

$$Z = \frac{T - T_\infty}{T_0 - T_\infty}, \tag{6}$$

where T_∞ and T_0 ar the free stream and initial sphere surface temperatures, respectively.

The conjugate problem takes into account the finite conductivity of the spherical particle. Since the sphere is solid, the energy transport of the interior may be modeled by a heat conduction equation written in dimensionless form as

$$\frac{\partial\hat{Z}}{\partial t} = \frac{2}{\hat{\mathrm{Pe}}}\left[\frac{\partial^2\hat{Z}}{\partial r^2} + \frac{2}{r}\frac{\partial\hat{Z}}{\partial r} + \frac{1}{r^2\sin\theta}\frac{\partial}{\partial\theta}\left(\sin\theta\frac{\partial\hat{Z}}{\partial\theta}\right)\right], \tag{7}$$

where $\hat{\mathrm{Pe}}$ is the Peclet number based on thermal diffusivity of the solid sphere and it represents a measure of the outside convection to the inside conduction. The dimensionless temperature $\hat{Z}$ is defined as in Eq. (6) except that T is replaced by $\hat{T}$. The superscript ^ indicates the interior of the sphere.

2.3. *Initial Conditions*

The sphere is assumed to be at a uniform temperature at $t = 0$. The thermophysical properties of the fluid and the sphere are assumed to be uniform initially and stay that way all the time. The flow is initially at rest at uniform temperatures. The mathematical representation of the above stated assumptions can be written as

$$\Psi(0, r, \theta) = 0, \Omega(0, r, \theta) = 0, Z(0, r, \theta) = 0, \hat{Z}(0, r, \theta) = 1. \tag{8}$$

2.4. *Flow Boundary Conditions*

The flow field's boundary conditions are the same as those in our previous work [2]. The flow field is assumed to be undisturbed by the presence of the sphere at a distance far from the sphere and the relative velocity between the fluid and the sphere is set to be zero at the sphere surface. These conditions, when imposed on the stream function and vorticity, amount to the constraints

$$\Psi(t, r, 0) = 0, \Psi(t, r, \pi) = 0, \Psi(t, 1, \theta) = 0 \tag{9}$$

$$\frac{\partial \Psi}{\partial r}(t, 1, \theta) = 0, \qquad \Omega(t, r \to \infty, \theta) \approx r^2 \int_{\mu}^{1} P_1(\mu^*)\, d\mu^*, \tag{10}$$

$$\Omega(t, r, 0) = 0, \qquad \Omega(t, r, \pi) = 0, \tag{11}$$

where $P_1(\mu)$ is the first-order Legendre polynomial.

2.5. *Temperature Boundary Conditions*

In this study, we prescribed two different boundary conditions. The one considers the conduction heat transfer dominant case at the sphere surface. For this case the heat flux and temperature continuity boundary conditions can be expressed as

$$\Phi_\kappa \frac{\partial \hat{Z}(t, 1, \theta)}{\partial r} = \frac{\partial Z(t, 1, \theta)}{\partial r} \tag{12}$$

$$\hat{Z}(t, 1, \theta) = Z(t, 1, \theta), \tag{13}$$

where Φ_κ is the ratio between the sphere and the fluid thermal conductivities (i.e., $= \hat{\kappa}/\kappa$ where $\hat{\kappa}$ is the sphere thermal conductivity and κ is the fluid thermal conductivity). In order to investigate the case of a nonlinear boundary condition, the other boundary condition we consider is that in which the conduction heat transfer balances with the sphere surface radiation energy transfer. In this case, the sphere is assumed to radiate the energy to the environment at temperature T_∞. In this case the heat flux boundary condition can be written as

$$\Phi_\kappa \frac{\partial \hat{Z}(t, 1, \theta)}{\partial r} = \frac{\partial Z(t, 1, \theta)}{\partial r} - N_r[1 - (1 - \Phi_T)\hat{Z}(t, 1, \theta)]^4, \tag{14}$$

where Φ_T $(= T_0/T_\infty)$ is the ratio of the initial temperature of the sphere to the far field temperature, and N_r is the alternate radiation–conduction number defined as

$$N_r = \varepsilon\sigma \frac{RT_\infty^4}{\kappa(T_0 - T_\infty)}. \tag{15}$$

Here ε is the surface emissivity and σ is the Stefan–Boltzmann constant. When the radiation heat flux is considered, the temperature continuity condition at the surface (i.e., Eq. (13)) is used with Eq. (15).

3. NUMERICAL METHOD

Following the previous paper [2], the full spectral method adopted in this study uses Chebyshev and Legendre polynomials as basis functions for series expansions in the radial and angular directions respectively. The detailed spectral formulation for stream function and vorticity has been given in a previous study [2], and will not be discussed further here. We will focus on the spectral formulation of the energy conservation equation.

3.1. *Spectral Representation of the Governing Equations*

The calculation domain is divided into two concentric spheres for which inner and outer domains represent the solid and the continuous phases respectively. The radial direction is made finite by projecting the outer region of the solid sphere, initially infinite, into a spherical shell whose normal distance between the two concentric spheres is further rescaled onto a new variable $\eta \in [-1, 1]$. This coordinate transformation is obtained by the use of an exponential mapping, which results in dense collocation points near the sphere surface where the velocity and temperature gradients are expected to be large. The inner region of the solid sphere is also transformed into a new variable $\xi \in [-1, 1]$. To be specific, this study uses the coordinate transformation

$$\begin{aligned} \eta &= 1 - \frac{2}{\eta_\infty} \log_e r \qquad && r > 1 \\ \xi &= 2r - 1 && r < 1, \end{aligned} \tag{16}$$

where η_∞ is a parameter large enough that the flow and temperature at any point with radius greater than $\exp(\eta_\infty)$ would behave like the free stream. The angular coordinate is mapped into a

new variable $\mu = \cos\theta$, so that we can expand the temperatures as a series of Legendre and associated Legendre polynomials; i.e.,

$$\{\hat{Z}(t, \xi, \mu), Z(t, \eta, \mu)\} = \sum_{n=0}^{NL} \{\hat{Z}_n(t, \xi), Z_n(t, \eta)\} P_n(\mu), \quad (17)$$

where $P_n(\mu)$ is the Legendre polynomial of order n, $P_n^1(\mu)$ is the associated Legendre polynomial of the first kind, and NL is the number of Legendre polynomials. By substituting Eq. (17) into Eqs. (4) and (7), and after considerable algebraic manipulation, the energy conservation equations for the outer and inner domains of the sphere become

$$\frac{\partial Z_n}{\partial t} = e^{-(1-\eta)\eta_\infty} \frac{2}{\mathrm{Pe}} \left[\frac{4}{\eta_\infty^2} \frac{\partial^2 Z_n}{\partial \eta^2} - \frac{2}{\eta_\infty} \frac{\partial Z_n}{\partial \eta} - n(n+1) Z_n \right] + S_n \quad (18)$$

$$\frac{\partial \hat{Z}_n}{\partial t} = \frac{8}{\hat{\mathrm{Pe}}} \left[\frac{\partial^2 \hat{Z}_n}{\partial \xi^2} + \frac{2}{1+\xi} \frac{\partial \hat{Z}_n}{\partial \xi} - \frac{n(n+1)}{(1+\xi)^2} \hat{Z}_n \right], \quad (19)$$

where S_n is the convection term which is written in spectral form as

$$S_n = e^{-5(1-\eta)\eta_\infty/4} \frac{1}{2} \sum_{j=0}^{NL} \sum_{i=1}^{NL} \left[\gamma_{ij}^n Z_j \left(\Psi_i - \frac{2}{\eta_\infty} \frac{\partial \Psi_i}{\partial \eta} \right) + \lambda_{ij}^n \Psi_i \frac{2}{\eta_\infty} \frac{\partial Z_j}{\partial \eta} \right]. \quad (20)$$

Here γ_{ij}^n and λ_{ij}^n are constants representing the integrals of three associated Legendre functions and may be shown to be given by

$$\lambda_{ij}^n = (2n+1) \begin{pmatrix} n & i & j \\ 0 & 0 & 0 \end{pmatrix} \begin{pmatrix} n & i & j \\ 0 & 0 & 0 \end{pmatrix} \quad (21)$$

$$\gamma_{ij}^n = -(2n+1) \left[\frac{j(j+1)}{i(i+1)} \right]^{1/2} \begin{pmatrix} n & i & j \\ 0 & 1 & -1 \end{pmatrix} \begin{pmatrix} n & i & j \\ 0 & 0 & 0 \end{pmatrix},$$

where $\begin{pmatrix} j_1 & j_2 & j_3 \\ m_1 & m_2 & m_3 \end{pmatrix}$ are the 3-J symbols. Rottenberg *et al.* [4] presented the theory expressing these symbols, and devised algorithms to compute them numerically.

Up to this point, Eqs. (18)–(20) are only partially spectral. In order to fully apply the spectral method to Eqs. (18) and (19), a series of Chebyshev polynomials is used to expand the temperatures in the remaining direction. By selecting the collocation points to be $\cos(i\pi/\mathrm{NT})$, where NT is the total number of collocation points, the solution becomes exact at those collocation points. The resulting expressions are written as

$$\frac{dZ_{nk}}{dt} = e^{-(1-\eta_k)\eta_\infty} \left[\sum_{l=0}^{NT} \left(\frac{4}{\eta_\infty^2} \hat{G}_{kl}^{(2)} - \frac{2}{\eta_\infty} \hat{G}_{kl}^{(1)} \right) Z_{nl} - n(n+1) Z_{nk} \right] + S_{nk} \quad (22)$$

$$\frac{\partial \hat{Z}_{nk}}{\partial t} = 4\Phi_\kappa \left[\sum_{l=0}^{NT_i} \left(\hat{G}_{kl}^{(2)} + \frac{2}{1+\xi_k} \hat{G}_{kl}^{(1)} \right) \hat{Z}_{nl} - \frac{n(n+1)}{(1+\xi_k)^2} \hat{Z}_{nk} \right], \quad (23)$$

where NT_i is the number of collocation points for the inner region of the sphere and S_{nk} becomes

$$S_{nk} = e^{-5(1-\eta_k)\xi_\infty/4} \frac{1}{2} \sum_{j=1}^{NL} \sum_{i=0}^{NL} \left[\gamma_{ij}^n Z_{ik} \left(\frac{1}{2} \Psi_{jk} - \frac{2}{\xi_\infty} \sum_{l=0}^{NT} \hat{G}_{kl}^{(1)} \Psi_{jl} \right) + \lambda_{ij}^n \Psi_{jk} \frac{2}{\xi_\infty} \sum_{l=0}^{NT} \hat{G}_{kl}^{(1)} Z_{il} \right], \quad (24)$$

where Z_{nk} and $\hat{Z}_{nk}$ refer to the nth component at the points η_k and ξ_k, respectively. Equations (22) and (23) are a system of mixed algebraic and differential equations which can be solved by various methods for initial value problems.

3.2. *Temporal Discretization*

The predictor–corrector and the multiple time levels, such as the combined second-order Adams–Bashforth and Crank–Nicholson algorithms, are the time differencing schemes commonly used in the spectral method. Although these schemes exhibit some desirable features in their own right, their applicability varies widely from problem to problem due to numerical instability arising from the explicitness. In the wake of such potential difficulty, we adopt a simple fully implicit scheme which, besides enhancing stability, enables us to use a relatively longer time step size. The implicit expressions for Eqs. (22) and (23) become

$$\frac{1}{\Delta t} Z_{nk}^{i+1} - e^{-(1-\eta_k)\eta_\infty} \left[\sum_{l=0}^{NT} \left(\frac{4}{\eta_\infty^2} \hat{G}_{kl}^{(2)} - \frac{2}{\eta_\infty} \hat{G}_{kl}^{(1)} \right) Z_{nl}^{i+2} - n(n+1) Z_{nk}^{i+1} \right] - S_{nk}^{i+1} = \frac{1}{\Delta t} Z_{nk}^{i} \quad (25)$$

$$\frac{1}{\Delta t} \hat{Z}_{nk}^{i+1} - 4\Phi_\kappa \left[\sum_{l=0}^{NT_i} \left(\hat{G}_{kl}^{(2)} + \frac{2}{1+\xi_k} \hat{G}_{kl}^{(1)} \right) \hat{Z}_{nl}^{i+1} - \frac{n(n+1)}{(1+\xi_k)^2} \hat{Z}_{nk}^{i+1} \right] = \frac{1}{\Delta t} \hat{Z}_{nk}^{i}, \quad (26)$$

where Δt is the time increment and the superscript i pertains to the time level.

Due to the nonlinear nature of Eqs. (25) and (26), it is inevitable that an iterative solution scheme be used. By repre-

senting the current time level, $i + 1$, as a variable without a superscript and assigning the superscript m as the iteration number at the given time level, Eqs. (25) and (26) can be recast as

$$\frac{1}{\Delta t} Z_{nk}^{m+1} - e^{-(1-\eta_k)\eta_\infty}\left[\sum_{l=0}^{\mathrm{NT}}\left(\frac{4}{\eta_\infty^2}\hat{G}_{kl}^{(2)} - \frac{2}{\eta_\infty}\hat{G}_{kl}^{(1)}\right) Z_{nl}^{m+1} - n(n+1) Z_{nk}^{m+1}\right] = S_{nk}^{m} + \frac{1}{\Delta t} Z_{nk}^{i} \tag{27}$$

$$\frac{1}{\Delta t}\hat{Z}_{nk}^{m+1} - 4\Phi_\kappa\left[\sum_{l=0}^{\mathrm{NT}i}\left(\hat{G}_{kl}^{(2)} + \frac{2}{1+\xi_k}\hat{G}_{kl}^{(1)}\right)\hat{Z}_{nl}^{m+1} - \frac{n(n+1)}{(1+\xi_k)^2}\hat{Z}_{nk}^{m+1}\right] = \frac{1}{\Delta t}\hat{Z}_{nk}^{i}. \tag{28}$$

Equations (27) and (28) are solved iteratively with updated flow information until convergence criteria are reached. The criteria for convergence are prescribed as

$$\begin{aligned} |Z_{nk}^{m+1} - Z_{nk}^{m}| &\le \varepsilon \qquad \forall\, n, k \\ |\hat{Z}_{nk}^{m+1} - \hat{Z}_{nk}^{m}| &\le \varepsilon \qquad \forall\, n, k, \end{aligned} \tag{29}$$

where ε is a prescribed tolerance. $\varepsilon = 10^{-4}$ is used throughout this work.

3.4. *Influence Matrix Technique*

The influence matrix technique is used to decompose the temperature as a linear combination of a set of auxiliary functions as

$$\begin{pmatrix} Z_n \\ \hat{Z}_n \end{pmatrix} = \begin{pmatrix} \zeta_0 \\ \hat{\zeta}_0 \end{pmatrix} + \beta_1 \begin{pmatrix} \zeta_1 \\ 0 \end{pmatrix} + \beta_2 \begin{pmatrix} 0 \\ \hat{\zeta}_1 \end{pmatrix}. \tag{30}$$

This technique has been used in a previous study [2] for decomposing the stream function and vorticity.

The expansion functions ζ_1 and $\hat{\zeta}_1$ are the solutions of the following supplementary problems:

$$\frac{1}{\Delta t}\zeta_{1k} - e^{-(1-\eta_k)\eta_\infty}\left[\sum_{l=0}^{\mathrm{NT}}\left(\frac{4}{\eta_\infty^2}\hat{G}_{kl}^{(2)} - \frac{2}{\eta_\infty}\hat{G}_{kl}^{(1)}\right)\zeta_{1l} - n(n+1)\,\zeta_{1k}\right] = 0 \tag{31}$$

$$\frac{1}{\Delta t}\hat{\zeta}_{1k} - 4\Phi_\kappa\left[\sum_{l=0}^{\mathrm{NT}i}\left(\hat{G}_{kl}^{(2)} + \frac{2}{1+\xi_k}\hat{G}_{kl}^{(1)}\right)\hat{\zeta}_{1l} - \frac{n(n+1)}{(1+\xi_k)^2}\hat{\zeta}_{1k}\right] = 0. \tag{32}$$

The boundary conditions which go along with the Eqs. (31) and (32) are

$$\left.\begin{aligned} \zeta_1(\eta = 1) &= 1 \\ \hat{\zeta}_1(\xi = 1) &= 1 \\ \zeta_1(\eta = -1) &= 0 \\ \left.\frac{d\hat{\zeta}_1}{d\xi}\right|_{\xi=-1} &= 0 \end{aligned}\right\}. \tag{33}$$

In order to meet all the requirements as specified in the original equations, the remaining auxiliary functions must be the solutions of the nonhomogeneous problems, the governing equations for ζ_0 and $\hat{\zeta}_0$; i.e.,

$$\frac{1}{\Delta t}\zeta_{0k} - e^{-(1-\eta_k)\eta_\infty}\left[\sum_{l=0}^{\mathrm{NT}}\left(\frac{4}{\eta_\infty^2}\hat{G}_{kl}^{(2)} - \frac{2}{\eta_\infty}\hat{G}_{kl}^{(1)}\right)\zeta_{0l} - n(n+1)\zeta_{0k}\right] = S_k + \frac{1}{\Delta t}\zeta_{0k} \tag{34}$$

$$\frac{1}{\Delta t}\hat{\zeta}_{0k} - 4\Phi_\kappa\left[\sum_{l=0}^{\mathrm{NT}i}\left(\hat{G}_{kl}^{(2)} + \frac{2}{1+\xi_k}\hat{G}_{kl}^{(1)}\right)\hat{\zeta}_{0l} - \frac{n(n+1)}{(1+\zeta_k)^2}\hat{\zeta}_{0k}\right] = \frac{1}{\Delta_t}\hat{\zeta}_{0k}. \tag{35}$$

Equations (34) and (35) are subjected to a homogeneous boundary condition which can be written as

$$\left.\begin{aligned} \zeta_0(\eta = 1) &= 0 \\ \hat{\zeta}_0(\xi = 1) &= 0 \\ \zeta_0(\eta = -1) &= 0 \\ \left.\frac{d\hat{\zeta}_0}{d\xi}\right|_{\xi=-1} &= 0 \end{aligned}\right\} \tag{36}$$

After solving for the Eqs. (32)–(36), it is necessary to calculate the decomposing coefficients β_1 and β_2 in order to obtain the desired temperatures. These coefficients are determined by satisfying the heat flux and temperature continuity conditions at the sphere surface. The boundary condition in Eqs. (12) and (13) leads to the following linear equations for the decomposing coefficients β_1 and β_2:

$$\beta_1 = \beta_2 = -\left(\frac{1}{\eta_\infty}\frac{d\zeta_0(1)}{d\eta} + \Phi_\kappa\frac{d\hat{\zeta}_0(1)}{d\xi}\right)\Big/\left(\frac{1}{\eta_\infty}\frac{d\zeta_1(1)}{d\eta} + \Phi_\kappa\frac{d\hat{\zeta}_1(1)}{d\xi}\right). \tag{37}$$

For the case in which radiation heat transfer is not negligible, Eqs. (15) and (13) reduce to

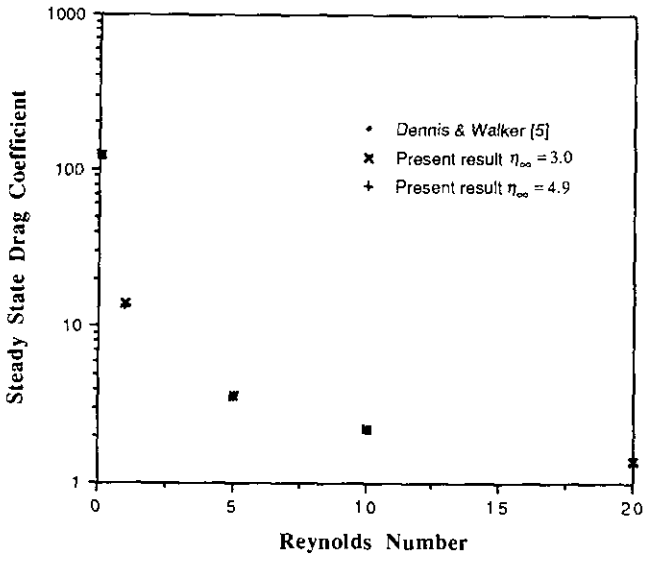

FIG. 2. Comparison of steady state drag coefficients.

$$N_t[1-(1-\Phi_T)]^4\beta_1^4 - \left[\frac{1}{\eta_\infty}\frac{d\zeta_1(1)}{d\eta} + \Phi_\kappa\frac{d\hat{\zeta}_1(1)}{d\xi}\right]$$
$$\beta_1 + \frac{1}{\eta_\infty}\frac{d\zeta_0(1)}{d\eta} - \Phi_\kappa\frac{d\hat{\zeta}_0(1)}{d\xi} = 0 \qquad (38)$$
$$\beta_1 = \beta_2.$$

Equation (38) is a nonlinear boundary condition which can be solved by using Newton's iterative scheme.

4. COMPARISONS WITH PREVIOUS RESULTS

In the following, more efforts to verify our numerical scheme have been directed to compare physical parameters calculated from the flow and temperature fields. Drag coefficients are calculated and compared with previous works as a means of verifying our approach. Results obtained in this study are compared with those of Dennis and Walker [5] for solid sphere calculations.

The drag coefficient C_d is defined as

$$C_d = \frac{D}{\pi\rho U_\infty^2 R^2}, \qquad (39)$$

where D is the drag force and ρ is the fluid density. The drag coefficient is composed of two parts, i.e., friction (D_f) and pressure (D_p) drags:

$$D_f = -4\pi\mu U_\infty R\int_0^\pi \omega_0 \sin^2\theta\, d\theta$$
$$D_p = -\pi R^2\int_0^\pi p_0 \sin 2\theta\, d\theta. \qquad (40)$$

ω_0 and p_0 are the vorticity and pressure on the surface of the sphere. The steady state values of drag coefficients are compared in Fig. 2 with varying η_∞ values. In general, present results are in excellent agreement with previous works within 0.5% error ranges.

Another comparison for the heat transfer calculation is given to Nusselt number calculations. The mean Nusselt number can be calculated as

$$Nu_m = -\int_0^\pi \frac{2}{\eta_\infty}\left(\frac{\partial Z}{\partial\eta}\right)_{\eta=0}\sin\theta\, d\theta. \qquad (41)$$

a constant sphere surface temperature boundary condition is used in order to make the results comparable with those obtained by Dennis *et al.* [7]. The Nusselt numbers are compared in Fig. 3 and are in good agreement. In all cases tested, the steady state calculations of both Nusselt number and drag coefficient compared the present model favorably with the previously published results.

5. RESULTS AND DISCUSSION

The flow and temperature fields at different time frames within and outside the solid sphere for the cases with Pr = 0.73 and Re = 10, 50, and 100 are shown in Figs. 4, 5, and 6, respectively. In the early stage, conduction is the dominant heat transfer mode, so the calculated isotherms show a nearly spherical shape for all Reynolds numbers considered (see Figs. 4a, 5a, and 6a. As time elapses, convection heat transfer becomes more influential so that the heat transfer is governed by both conduction and convection. The resulting isotherms show that the thermally affected zones are shifted toward the downstream direction of the flow. For the high Reynolds number cases, i.e., Figs. 5 and 6, the recirculation zones are developed behind the sphere at 3 units of dimensionless time. Because

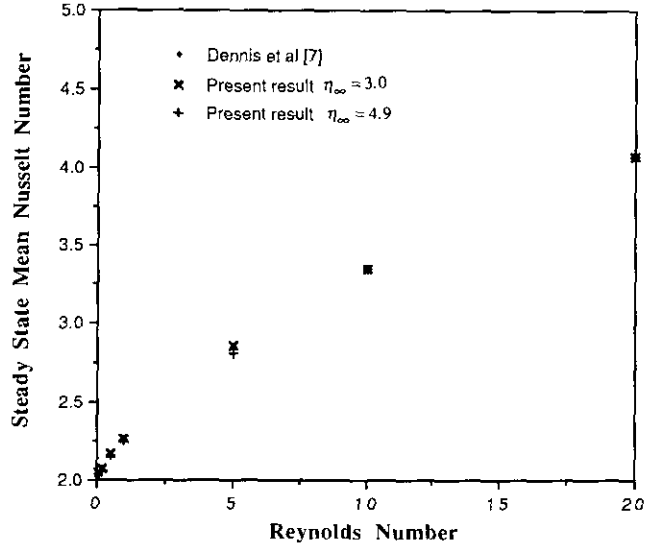

FIG. 3. Comparison of steady state Nusselt number.

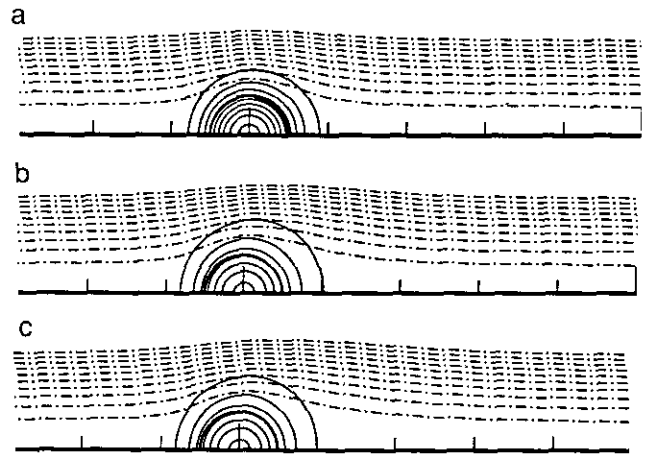

FIG. 4. Streamlines (dashled line) and isotherms (solid line) for a solid sphere with Re = 10 and Pr = 0.73 at (a) t = 1.0, (b) t = 3.0, (c) t = 5.0.

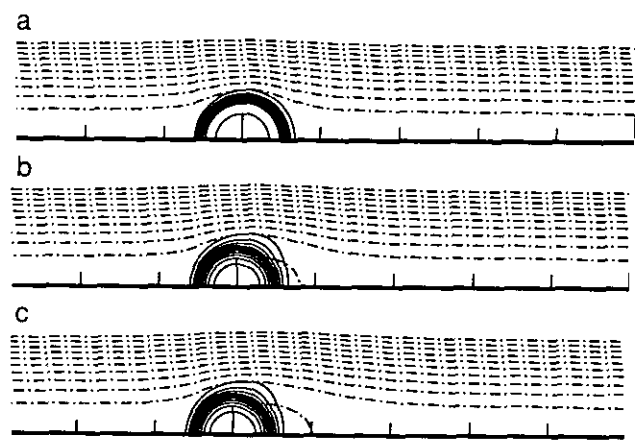

FIG. 6. Streamlines (dashed line) and isotherms (solid line) for a solid sphere with Re = 5 and Pr = 0.73 at (a) t = 1.0, (b) t = 3.0, (c) t = 5.0.

of the recirculation zones where the velocities are small, the resulting isotherms near the sphere show a plateau around the area. This effect becomes stronger as time passes (see Figs. 5c and 6c). It is interesting to note that for high Reynolds number cases steeper temperature gradients develop near the surface than those for low Reynolds number cases. This is because in high Reynolds number cases, the resulting Peclet number is high for a fixed Prandtl number. Thus the temperature profile near the trailing edge of the sphere shows the pattern of high Peclet number cases (Pe = Re Pr). As expected, in the low Reynolds number cases the thermally affected zone stretches more in the direction perpendicular to the flow direction than it does in the high Reynolds number cases.

The accuracy of the quasi-steady assumption, i.e., the assumption that uses the steady state flow field and solves transient energy equations for the temperature field, is tested by checking the Nusselt number values with the fully transient solution approach in both flow and temperature fields. Figure 7 shows the degree of underprediction using quasi-steady assumption as compared to the fully transient solution. The error is defined as the percentage of the Nusselt number difference to the fully transient Nusselt number. The steady-state flow field is obtained after 20 units of dimensionless time has elapsed. The same energy conservation equation is solved for both the quasi-steady and the fully transient approaches. It is found that the Nusselt number obtained by the fully transient approach gives higher values than those obtained by quasi-steady assumption. This is because in the early time periods of the fully transient situation the momentum boundary layer near the sphere surface is not developed, resulting in steeper velocity and temperature

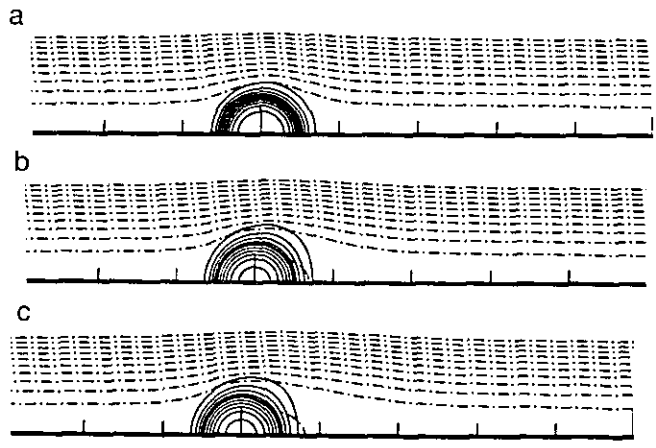

FIG. 5. Streamlines (dashed line) and isotherms (solid line) for a solid sphere with Re = 50 and Pr = 0.73 at (a) t = 1.0, (b) t = 3.0, (c) t = 5.0.

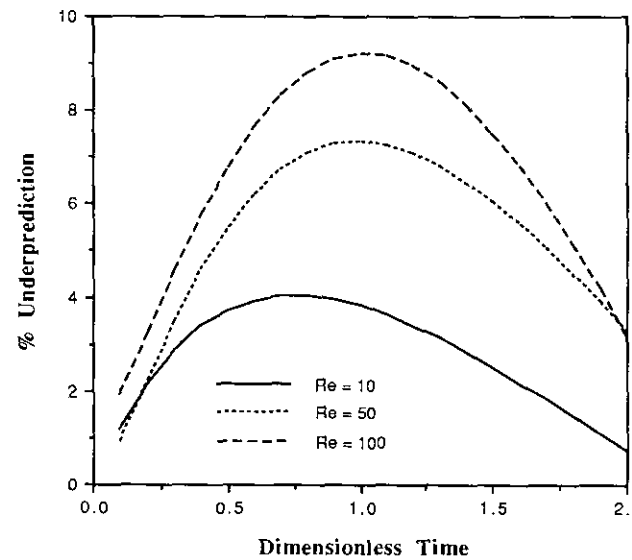

FIG. 7. Percent underprediction of quasi-steady results for the transient Nusselt number.

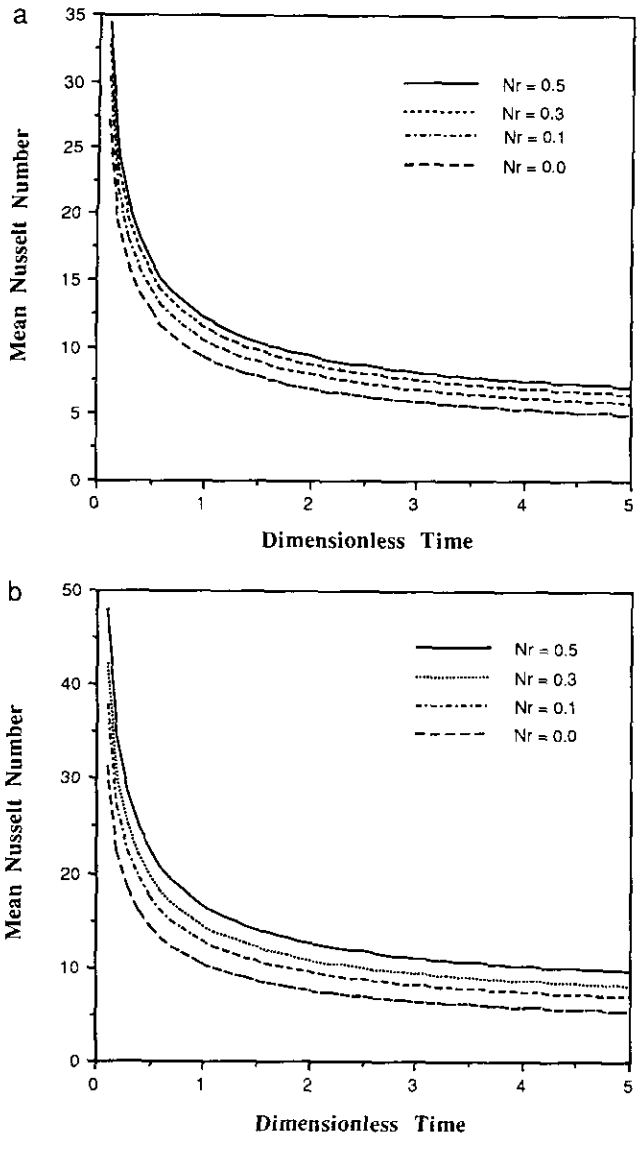

FIG. 8. Transient Nusselt number for different values of N_r for (a) Re = 50 and (b) Re = 100.

gradients than those calculated using the quasi-steady assumption at the same time scale. The development of thermal and momentum boundary layers near the sphere surface becomes significant as time elapses so that the steep gradients smear out over the external fields, which results in a small discrepancy for these two different cases. The quasi-steady analyses performed in this study for different Peclet numbers give results similar to those of Abramzon and Borde [9]. It is also interesting that, as the Reynolds number increases, the discrepancy between quasi-steady and fully transient calculations becomes larger.

The results of using the radiation heat flux boundary are shown in Fig. 8. Pr = 0.73 is used for the both the Re = 50 (Fig. 8a) and the Re = 100 (Fig. 8b) cases. These curves indicate that the heat transfer increases as the N_r increases. This is expected because the strong surface radiation results in a higher heat flux from the sphere surface [10].

6. CONCLUSIONS

In this study, a Chebyshev–Legendre spectral method is successfully adopted for a solution scheme of the heat transfer problem from a solid sphere with linear and nonlinear boundary conditions at the sphere surface. Presented results show cases for the Reynolds number up to 100. Even though the present numerical schemes are applicable for higher Reynolds number cases than presented, the results for the higher Reynolds number cases are not studied in this work because of the excessive memory requirements for those cases.

The nonlinear boundary condition arising from the radiation heat transfer is treated successfully by using Newton's iterative scheme. It is found that for a given Prandtl number, the underprediction of quasi-steady assumption increases as the Reynolds number increases. The discrepancy between the quasi-steady and the fully transient treatments of the flow fields diminishes as time elapses.

ACKNOWLEDGMENTS

The authors thank Dr. R. W. Douglass for his valuable comments and Dr. M. J. Oliver and Mr. V. A. Mousseau for their assistance in running the computer program. This work was performed under the auspices of the U.S. Department of Energy, Contract DE-AC07-76-ID01570.

REFERENCES

1. R. Clift, J. C. Grace, and M. E. Weber, *Bubbles, Drops, and Particles* (Academic Press, New York, 1978).
2. H. D. Nguyen and J. N. Chung, *J. Comp. Phys.* **104,** No. 2, 303 (1991).
3. C. L. Lin and S. C. Lee, *Computers and Fluids* **1,** 235 (1973).
4. M. Rottenberg, R. Bivins, N. Metropolis, and J. K. Wooten, *The 3-J and 6-J Symbols* (MIT Press, Cambridge, MA, 1959).
5. S. C. R. Dennis and J. D. A. Walker, *J. Fluid Mech.* **48,** 771 (1971).
6. D. L. R. Oliver and J. N. Chung, *J. Fluid Mech.* **154,** 215 (1985).
7. S. C. R. Dennis, J. D. A. Walker, and J. D. Hudson, *J. Fluid Mech.* **60,** 273 (1973).
8. S. C. R. Dennis and J. D. A. Walker, *Phys. of Fluids* **15,** 517 (1972).
9. B. Abramzon and I. Borde, *AIChE J.* **26,** 536 (1980).
10. H. D. Nguyen and A. Azia, *Wärme- und Stoffübertragung* **67,** 678 (1992).